Observation of Quantum Interference between Separated Mechanical Oscillator Wave Packets

D. Kienzler, C. Flühmann, V. Negnevitsky, H.-Y. Lo, M. Marinelli, D. Nadlinger, and J. P. Home*
Institute for Quantum Electronics, ETH Zürich, Otto-Stern-Weg 1, 8093 Zürich, Switzerland
(Received 26 January 2016; published 5 April 2016)

We directly observe the quantum interference between two well-separated trapped-ion mechanical oscillator wave packets. The superposed state is created from a spin-motion entangled state using a heralded measurement. Wave packet interference is observed through the energy eigenstate populations. We reconstruct the Wigner function of these states by introducing probe Hamiltonians which measure Fock state populations in displaced and squeezed bases. Squeezed-basis measurements with 8 dB squeezing allow the measurement of interference for $\Delta\alpha = 15.6$, corresponding to a distance of 240 nm between the two superposed wave packets.

DOI: 10.1103/PhysRevLett.116.140402

The rules of quantum mechanics give rise to the prediction that systems can exist in a superposition of two macroscopically distinct quantum states, connected by a fixed relationship known as the quantum phase. This is illustrated by the Schrödinger's cat thought an experiment in which a cat is envisioned as being simultaneously dead and alive, a situation which has no counterpart in our classically familiar world. The key distinction which separates the quantum superposition from a classical mixture is the phase relationship between the two distinct parts of the superposition. An approximation to such a situation is provided by superposed "classical" coherent states of oscillators which are macroscopically distinct at large amplitudes. Such "cat" states have been realized in the oscillations of trapped atomic ions [1–6], and for the electromagnetic field [7,8]. While the direct phase relationship between the two states has been observed for the latter, for massive particles (such as trapped ions and matter-wave interferometers [9]) in which spatial superpositions have been created, no *in situ* measurements have been performed. Quantum coherence has instead been verified by bringing the two separated wave packets together so that they spatially overlap and observing the resulting revival of coherence [1,6]. For large cat sizes, both the mean and the uncertainty in energy of the superposed wave packets is increased. As viewed from the energy eigenbasis, the states occupy an increasingly large Hilbert space, and thus become progressively harder to characterize. This provides an additional challenge to experiments which seek to probe cat states in the mesoscopic regime.

In this Letter, we use an in-sequence spin measurement on a spin-motion entangled state to project out and herald a superposition of two coherent mechanical oscillator states of opposite phases. We perform measurements which directly observe the interference of the two spatially separated wave packets through the effect on the occupation of the energy eigenstates. For $\alpha > 5$ the standard analysis method, which is based on an energy eigenstate decomposition, has a poor signal to noise ratio. We overcome this limitation by performing an analogous eigenstate decomposition in a squeezed Fock basis in which the mean quantum number of the cat is reduced substantially. Using a Fock basis with 8 dB of squeezing, we are able to observe quantum interference for phase-space separations of $\Delta\alpha = 15.6$, which correspond to a direct measurement of interference between wave packets separated by 240 nm with a root-mean-square extent of 7.8 nm. Adding an extra term to the probe Hamiltonian, we displace the analysis basis, providing a method for reconstructing the Wigner function of the oscillator state. We demonstrate a full reconstruction using the nonsqueezed basis for a cat with $\alpha = 2.1$, and we take additional slices through the phase space for cats with $\alpha = 4.25$ and 5.9, making use of a squeezed analysis basis with 7 dB of squeezing for the larger state.

The oscillator cat states are experimentally generated using a single motional mode of a trapped $^{40}Ca^{+}$ ion, which can be treated as a mechanical harmonic oscillator with a frequency of $\omega_m \approx 2\pi \times 2.08$ MHz. We implement a two-level pseudospin using the ion's electronic transition $|L=0, J=1/2, M_J=+1/2\rangle \leftrightarrow |L'=2, J'=5/2, M'_J=3/2\rangle$, which we label with $|\downarrow\rangle$ and $|\uparrow\rangle$, respectively. We couple the two levels using a narrow-linewidth laser with a wavelength of 729 nm and a k vector at an angle of 45° to the ion's axis of motion, resulting in a Lamb-Dicke parameter of $\eta \approx 0.05$ (more details on the experimental methods can be found in the Supplemental Material [10]). Starting from an ion prepared in $|\downarrow\rangle$ and the oscillator ground state, we apply an internal-state dependent force using a Hamiltonian $\hbar\Omega\hat{\sigma}_x(\hat{a}^\dagger + \hat{a})/2$, where $\hat{\sigma}_x = |+\rangle\langle+| - |-\rangle\langle-|$, with $|\pm\rangle \equiv (|\downarrow\rangle \pm |\uparrow\rangle)/\sqrt{2}$, and Ω is a constant. In our experiments this is well approximated by simultaneously driving the red and blue motional sidebands of the internal-state transition $|\downarrow\rangle \leftrightarrow |\uparrow\rangle$ [1] (corrections

due to higher order terms in the laser-ion interaction are relatively small—see the Supplemental Material [10] for more information). After applying this Hamiltonian for a duration t, the state of the ion can ideally be written as a spin-motion entangled state,

$$|\psi_{\mathrm{ent}}\rangle = \frac{1}{\sqrt{2}}(|+\rangle|\alpha\rangle + |-\rangle|-\alpha\rangle), \tag{1}$$

where $\alpha = -i\Omega t/2$ relates the amplitude of oscillation z to the rms extent of the ground state wave function z_0 via $z = 2\alpha z_0$. This is the standard cat state which has been produced in earlier work with trapped ions [1–3,5], in which the superposed motional wave packets are separated in phase space by $\Delta\alpha = 2\alpha$ but are entangled with the ion's internal state. $|\psi_{\mathrm{ent}}\rangle$ can be written in the $|\uparrow\rangle$, $|\downarrow\rangle$ basis as

$$|\psi_{\mathrm{ent}}\rangle = \frac{1}{\sqrt{2}}(|\uparrow\rangle|\psi_-\rangle + |\downarrow\rangle|\psi_+\rangle), \tag{2}$$

where $|\psi_\pm\rangle \equiv (|\alpha\rangle \pm |-\alpha\rangle)/\sqrt{2}$. A measurement of the internal state therefore projects the motional state into a superposition of two out-of-phase oscillations, with the quantum phase relating the two depending on the measurement result. Detection of the internal state involves applying a resonant laser which scatters many photons for the $|\downarrow\rangle$ state, but none for the $|\uparrow\rangle$ state [12]. The former results in photon recoil which destroys the motional state; thus, we make an in-sequence decision to only proceed with the analysis of the motional state when the internal state is found to be $|\uparrow\rangle$. The state $|\psi_+\rangle$ ($|\psi_-\rangle$) contains only even (odd) energy eigenfunctions due to the quantum interference between the two coherent states $|\pm\alpha\rangle$. The state populations $p(|n\rangle)$ are extracted by observing the spin projection as a function of the duration t_p of a probe Hamiltonian $\hat{H}_r = (\hbar\Omega_r/2)[\hat{a}^\dagger\hat{\sigma}_- + \mathrm{H.c.}]$. Experimentally, this Hamiltonian is realized by driving the red-sideband transition $|\uparrow, n\rangle \leftrightarrow |\downarrow, n+1\rangle$. The probability of observing spin $|\downarrow\rangle$ after the pulse follows

$$P(\downarrow, t_p) = \frac{1}{2}\sum_n p(|\phi_n\rangle)[1 - \gamma(t)\cos(\Omega_{n,n+1}t_p)], \tag{3}$$

where $p(|\phi_n\rangle)$ is the probability that the motion started in the Fock state $|\phi_n\rangle$ prior to the probe pulse. When using the red-sideband probe, these Fock states correspond to the energy eigenstates $|\phi_n\rangle = |n\rangle$ and the Rabi frequencies $\Omega_{n,n+1} = \Omega_r M_n$ scale with n according to the motional matrix elements $M_n = \langle n+1|e^{i\eta(\hat{a}^\dagger+\hat{a})}|n\rangle$. For small values of the dimensionless Lamb-Dicke parameter η, these scale as $\sqrt{n+1}$ [13]. $\gamma(t)$ accounts for decay in the coherence of the whole system during the probe pulse. In fitting data, we use a phenomenological exponential decay $\gamma(t) = e^{-\Gamma t}$ (more details on the fits can be found in the Supplemental Material [10]). Data obtained using this method are shown for three states with $|\alpha| \simeq 3$ in Fig. 1, alongside the motional populations obtained from fits of Eq. (3) to the data. In the first, we do not perform a postselected measurement but rather probe the motional state populations after repumping to $|\downarrow\rangle$, resulting in the density matrix $\hat{\rho}_{\mathrm{mix}} = (|\alpha\rangle\langle\alpha| + |-\alpha\rangle\langle-\alpha|)/2$, which has a Poisson population distribution of energy eigenstates [this leaves the ion in $|\downarrow\rangle$, and thus, in contrast to all other measurements in this Letter, we probe using the Hamiltonian $\hat{H}_b = (\hbar\Omega_b/2)[\hat{a}^\dagger\hat{\sigma}_+ + \mathrm{H.c.}]$, implemented by driving the blue sideband $|\downarrow, n\rangle \leftrightarrow |\uparrow, n+1\rangle$, resulting in a spin probability $P'(\downarrow, t_p) = 1 - P(\downarrow, t_p)$]. The photon recoil from the repumping step leads to the emission of less than three photons, on average, and reduces the fidelity of the final state by around 2%. The time evolution of the spin populations shows the well-known collapse and revival, with the latter occurring when Rabi oscillations for neighboring values of n come into phase [14]. This occurs around $t_{r,\mathrm{mix}} \simeq 4\pi/[\Omega_r(\sqrt{\langle n\rangle + 1} - \sqrt{\langle n\rangle})]$, corresponding to $t_{r,\mathrm{mix}} = 386\ \mu\mathrm{s}$ for the settings $\Omega_r/(2\pi) = 31$ kHz and $\bar{n} = |\alpha|^2 = 8.76$ used in our experiment. The results for

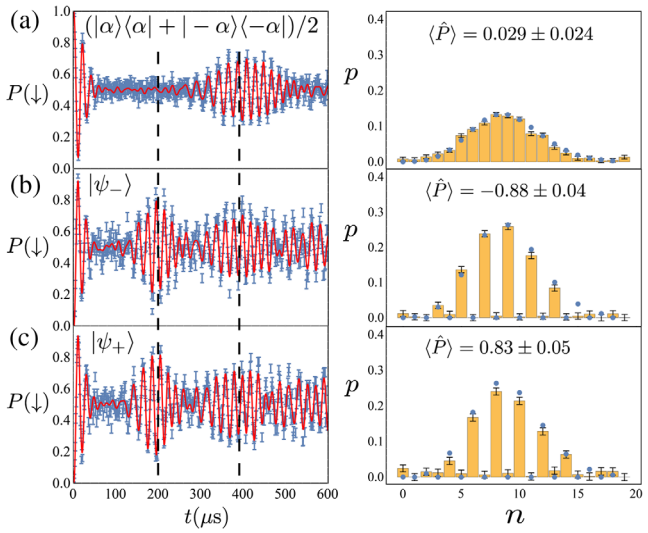

FIG. 1. Experimental data from measurements of $P(\downarrow, t_p)$ using $\hat{H}_r$ [$\hat{H}_b$ for (a)] (left panels), fitted using Eq. (3) to obtain the motional energy eigenstate populations (right panels). The data are taken by preparation of state $|\psi_{\mathrm{ent}}\rangle$, followed by an analysis which is performed after (a) repumping the spin to $|\downarrow\rangle$, (b) detection of the ion in the state $|\uparrow\rangle$, producing the state $|\psi_-\rangle$, and (c) detection of the ion in the state $|\uparrow\rangle$ after applying a spin flip using the carrier transition, which produces $|\psi_+\rangle$. The vertical dashed lines indicate the revival times t_r and $t_{r,\mathrm{mix}}$. The reconstructed population distributions show the effect of the postselected measurement for the latter two cases. The blue points in the population graphs correspond to the ideal cases for $\alpha = 3$. Spin populations are the result of 250 repeats of the full experimental sequence, which corresponds to roughly 125 analysis detections for the postselected cases. Error bars are estimated from quantum projection noise. The population errors are given as the standard error of the mean (SEM).

the mixed state should be compared with cases in which the states are analyzed conditionally to the results of a spin measurement of the internal state. The first corresponds to analyzing the motional state only when the spin is measured to be $|\uparrow\rangle$, which ideally produces $|\psi_-\rangle$. For the second, we perform a coherent spin inversion prior to the conditional measurement, which ideally projects the motion into $|\psi_+\rangle$. For both $|\psi_+\rangle$ and $|\psi_-\rangle$, the revival at $t_p = t_{r,\mathrm{mix}}$ is accompanied by an additional revival in the spin population oscillations at around 198 μs, which results from a rephasing of the contributions from Fock states differing in n by 2. This corresponds to the condition $t_r = 4\pi/[\Omega_r(\sqrt{\langle n\rangle + 2} - \sqrt{\langle n\rangle})]$, which, for $\langle n\rangle \gg 2$, gives $t_r \simeq 4\pi\sqrt{\langle n\rangle}/\Omega_r \simeq t_{r,\mathrm{mix}}/2$. We see in the populations extracted from the fit that the odd and even cat states contain predominantly odd or even number states. We use these populations to extract the parity $\langle\hat{P}\rangle \equiv \sum_n (-1)^n p(|n\rangle)$ of the number state distributions, obtaining 0.029 ± 0.024 for the mixture, -0.88 ± 0.04 for $|\psi_-\rangle$, and 0.83 ± 0.05 for $|\psi_+\rangle$.

In the methods used above, the visibility of the revival of oscillations in the spin population at time t_r is the key element for diagnosing the parity of the cat. Since the mean Rabi rate scales as $\sqrt{\langle n\rangle + 1}$, the revival time corresponds to approximately $\langle n\rangle$ Rabi oscillations on the motional sideband. In order to observe a significant revival, this time must be short compared to relevant decoherence times for the cat state, and the stability of the Rabi oscillations must be high enough that $\langle n\rangle$ oscillations are visible for all relevant Fock states. The coherence time of trapped-ion oscillator cats due to motional heating and motional dephasing scales roughly as $1/|\Delta\alpha|^2$ [15], and we observe that our spin-motion Rabi oscillations decay with a time constant which is proportional to the Rabi frequency (see the discussion in the Supplemental Material [10]).

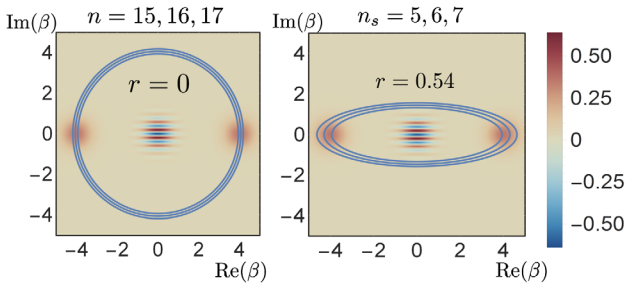

FIG. 2. Comparison between the energy eigenbasis and the squeezed basis for $\alpha = 4$ and $r = 0.54$. The Wigner function of the cat state is overlayed by lines which indicate the maximal quasiprobability of the three closest Fock states to the mean value of the cat state in the relevant basis. This is approximately given by $\beta = (n + 1/2)^{1/2}[\cos(\theta)e^r + i\sin(\theta)e^{-r}]$ [17]. The use of the squeezed basis reduces both the mean value and the variance, simplifying the extraction of the motional populations from the spin oscillation data.

The combination of these two effects means that we are unable to observe an interference feature for a cat with $\Delta\alpha \gtrsim 10$. To overcome this problem, we introduce an analysis method based on a squeezed Fock state basis $|\phi_{n_s}\rangle = |n_s\rangle \equiv \hat{S}(\xi)|n\rangle$, where the squeezing operator is defined as $\hat{S}(\xi) \equiv e^{(\xi^*\hat{a}^2 - \xi\hat{a}^{\dagger 2})/2}$, with $\xi \equiv re^{i\phi_s}$ [16]. The basic idea is illustrated in Fig. 2. We choose the squeezing axis perpendicular to the axis separating the two wave packets of the cat, which corresponds to selecting the phase $\phi_s = 2\arg\alpha + \pi$. The effect of the antisqueezing results in a mean occupation in the squeezed basis of $\langle n_s\rangle = |\alpha|^2 e^{-2r} + \sinh^2(r)$, exponentially suppressing the contribution from the displacement at the cost of an additional contribution which can be kept small with an appropriate choice of r. The minimum value of $\langle n_s\rangle$ for a given α is reached for $r_{\min} = \ln(4|\alpha|^2 + 1)/4$. Since the squeezing operator preserves parity, the even (odd) cats consist of only even (odd) number state populations in both bases.

To measure our states in the squeezed basis, we substitute the Hamiltonian $\hat{H}_s \equiv (\hbar\Omega_s/2)[(\hat{a} + \tanh(r)e^{i\phi_s}\hat{a}^\dagger)\hat{\sigma}_- + \mathrm{H.c.}]$ for $\hat{H}_r$, which is implemented in the experiment by adding a second frequency to the probe laser pulse, with a frequency $2\omega_m$ lower than the blue-sideband component (making it resonant with the red sideband) and with its amplitude reduced relative to the blue sideband by a factor $\tanh(r)$ (for the calibration of the phases, see the Supplemental Material [10]). The time evolution of the spin populations follows Eq. (3), with the relevant number states becoming those of the squeezed basis. In the Lamb-Dicke regime the scaling of the Rabi frequencies is again $\sqrt{n_s + 1}$, though in fitting the data we use values for the matrix elements which include higher order terms. Data for cat states with $|\alpha| = 6.6$, 7.15, and 7.8 are shown in Fig. 3. The optimal choice of r for minimizing $\langle n_s\rangle$ was not used because we observe that, for a larger r, the Rabi oscillations of the squeezed Hamiltonian dephase, which impedes the signal. This is a consequence of the squeezed basis' increased sensitivity to the dephasing of the motional state compared to the standard analysis. In addition, we do not gain the full speedup in the revival time because, in our setup, $\Omega_s < \Omega_r$. Nevertheless, for our largest cat the number of Rabi oscillations at which the revival occurs is reduced from 60 to 11, which is essential for observing the interference. By fitting Eq. (3) with floated number state populations, we obtain the results shown in Fig. 3, from which we extract parities of $\langle\hat{P}\rangle = -0.55 \pm 0.03$, -0.48 ± 0.03, and -0.30 ± 0.03 for $|\alpha| = 6.6$, $|\alpha| = 7.15$, and $|\alpha| = 7.8$, respectively. Also shown in Fig. 3 are the populations obtained from a fit to the experimental $P(\downarrow, t_p)$ using a model of the motional populations which is derived from a weighted sum of the even and odd cats, $\hat{\rho}_{\mathrm{mix}} = \xi_{\mathrm{mix}}|\psi_-\rangle\langle\psi_-| + (1 - \xi_{\mathrm{mix}})|\psi_+\rangle\langle\psi_+|$. The close match between theory and experiment indicates that the primary

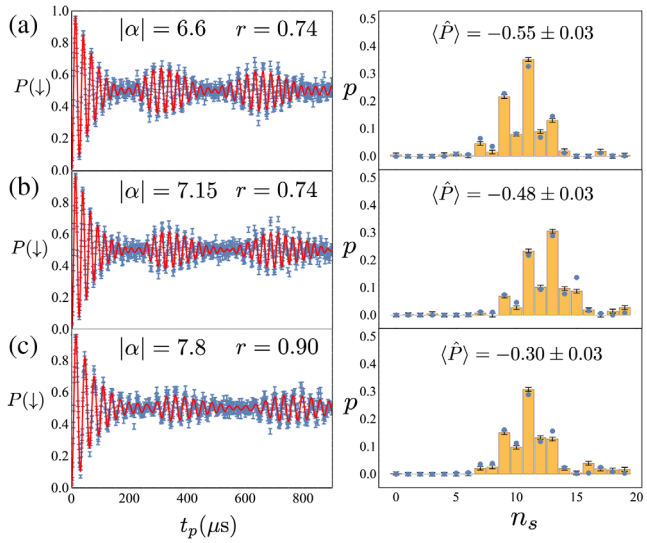

FIG. 3. Experimental data for the spin evolution $P(\downarrow, t_p)$ obtained by probing in the squeezed basis with $\hat{H}_s$ (left panels). These are fitted by using Eq. (3) to obtain the squeezed Fock state populations (right panels). The parameters for the cat size and the squeezing amplitude are given, along with the parity value obtained from the extracted populations. The blue points in the Fock state population plots are the populations obtained from a fit using a weighted mixture of $|\psi_+\rangle$ and $|\psi_-\rangle$. Experimental data points are an average of 750 repeats of the full experimental sequence for (a) and (b) [1000 for (c)], which corresponds to roughly 375 (500) analysis detections for the postselected cases. Error bars are estimated from quantum projection noise. Errors on population and parity estimates are given as the SEM.

decoherence mechanism mixes the two cat states, which is compatible with heating of the ion due to fluctuations in the electric field at frequencies close to the ion's oscillation frequency [15,18].

The Wigner function is a phase-space quasiprobability distribution which plays an important role in visualizing and characterizing oscillator states [17]. It can be related to the expectation value of the parity operator for the populations of displaced number states with displacement β as $W(\beta) = 2/\pi\langle\hat{P}(\beta)\rangle$, with $\langle\hat{P}(\beta)\rangle = \sum_n (-1)^n p(\hat{D}(\beta)|n\rangle)$ and $\hat{D}(\beta) \equiv e^{\beta\hat{a}^\dagger - \beta^*\hat{a}}$ the displacement operator [8,19]. This relationship has previously been used to experimentally reconstruct motional states of a trapped-ion oscillator using a method that involves displacing the state by $-\beta$, followed by extraction of the populations in the energy eigenstate basis [19]. Rather than taking this approach, we obtain the populations of the oscillator states directly in the displaced basis, by adding a displacement term $\hat{H}_d(\beta) = \hbar\Omega/2(\beta^*\hat{\sigma}_+ + \beta\hat{\sigma}_-)$ to the Hamiltonian used to probe the state [16]. We do this for both $\hat{H}_r$ and $\hat{H}_s$ by adding a laser component resonant with the carrier transition $|\uparrow\rangle \leftrightarrow |\downarrow\rangle$, with Ω chosen to equal Ω_r and Ω_s for each case. Under the action of the modified Hamiltonian, the spin population dynamics follow Eq. (3), but with the relevant probabilities being those of the displaced number states $|\phi_n\rangle = \hat{D}(\beta)|n\rangle$ or the displaced squeezed number states $\hat{S}(\xi)\hat{D}(\beta)|n\rangle$ [10,16].

The reconstructed Wigner function for an odd cat state with $\alpha \simeq 2.1$ is shown in Fig. 4, based on number state population extraction using Eq. (3) on a grid of 17×21 values of β. This shows the expected features, including the two separated peaks corresponding to the coherent state wave packets as well as the interference fringes close to $\beta = 0$. Results are also shown for cuts along the imaginary axis of phase space for a cat with $\alpha \simeq 4.25$, extracted using measurements in both the energy eigenstate basis and a squeezed basis with $r = 0.5$. We fit the functional form $f(x) = 2/\pi A e^{-2x^2}\cos(4\alpha x)$ with $x = \mathrm{Im}(\beta)$ [14], and we extract $\alpha = 4.21 \pm 0.02$ and $A = 0.90 \pm 0.02$ for the unsqueezed basis and $\alpha = 4.25 \pm 0.02$ and $A = 1.00 \pm 0.03$ for the squeezed basis. Also shown is similar data for a cat with $\alpha \simeq 5.9$, which were taken using a displaced-squeezed probe Hamiltonian with $r = 0.8$. In this case the fitted curve gives $\alpha = 5.86 \pm 0.02$ and $A = 0.57 \pm 0.01$.

The ability to project the ion into a superposition of different locations and to directly measure the interference of these states allows probing of the cat coherence free from entanglement with the microscopic spin, which is advantageous for probing the limits of quantum coherence in these systems. The use of a squeezed basis in tomographic reconstructions may provide advantages for reconstructing a range of quantum states with large

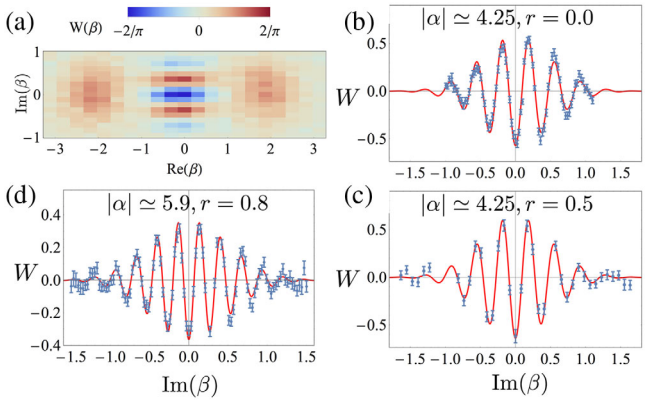

FIG. 4. Reconstructed Wigner functions (a) for a cat with $\alpha \simeq 2.0$, extracted using 289 settings of the displaced Fock state basis, (b) on the imaginary axis in phase space for a cat with $\alpha = 4.2$, using a displaced basis, (c) for $\alpha \simeq 4.3$ performed using a displaced-squeezed basis with $r = 0.5$, (d) for a cat with $\alpha \simeq 6$ performed using a displaced-squeezed basis with $r = 0.8$. In (b)–(d) the fits are a theoretical form which can be derived from the Wigner function of a well-separated cat state (for further details, see the Supplemental Material [10]). Errors bars are given as the SEM. The $\mathrm{Im}(\beta)$ axis is extracted from periodic calibration scans, and we observe drifts in the scaling at the 10% level over a day. Thus there is some uncertainty in the values of $\mathrm{Im}(\beta)$ due to drifts between calibrations.

phase-space amplitudes. In the work above, it allows the reduction of a state with a mean occupancy of around 60 quanta to one which has a mean of 11. These methods should be applicable in a range of systems in which similar spin-oscillator couplings are available, including other mechanical oscillators which might be used to probe gravitational or nonlinear collapse theories in quantum physics [20,21]. The measurement technique used to create the states in the work here is suitable for performing tests of macroscopic realism based on Leggett-Garg inequalities [22].

Recently, we became aware of parallel work in which a direct parity measurement is used to measure cat states produced in a similar manner using a single motional mode of a two-ion crystal [23].

We thank Lukas Gerster, Ludwig de Clercq, and Ben Keitch for their contributions to the experimental apparatus. We acknowledge support from the Swiss National Science Foundation under Grant No. 200020_153430 and through the National Centre of Competence in Research for Quantum Science and Technology (QSIT), and from ETH Research Grant No. ETH-18 12-2.

*Corresponding author.
jhome@phys.ethz.ch

[1] C. Monroe, D. M. Meekhof, B. E. King, and D. J. Wineland, Science **272**, 1131 (1996).
[2] P. C. Haljan, P. J. Lee, K.-A. Brickman, M. Acton, L. Deslauriers, and C. Monroe, Phys. Rev. A **72**, 062316 (2005).
[3] M. J. McDonnell, J. P. Home, D. M. Lucas, G. Imreh, B. C. Keitch, D. J. Szwer, N. R. Thomas, S. C. Webster, D. N. Stacey, and A. M. Steane, Phys. Rev. Lett. **98**, 063603 (2007).
[4] U. Poschinger, A. Walther, K. Singer, and F. Schmidt-Kaler, Phys. Rev. Lett. **105**, 263602 (2010).
[5] D. J. Wineland, Rev. Mod. Phys. **85**, 1103 (2013).
[6] H.-Y. Lo, D. Kienzler, L. de Clercq, M. Marinelli, V. Negnevitsky, B. Keitch, and J. Home, Nature (London) **521**, 336 (2015).
[7] S. Haroche, Rev. Mod. Phys. **85**, 1083 (2013).
[8] B. Vlastakis, G. Kirchmair, Z. Leghtas, S. E. Nigg, L. Frunzio, S. M. Girvin, M. Mirrahimi, M. H. Devoret, and R. J. Schoelkopf, Science **342**, 607 (2013).
[9] M. Kasevich and S. Chu, Phys. Rev. Lett. **67**, 181 (1991).
[10] See Supplemental Material at http://link.aps.org/supplemental/10.1103/PhysRevLett.116.140402, which includes Ref. [11], for the experimental setup, initial state preparation, heralding detection, corrections to the Lamb-Dicke approximation, discussion of the decay model and observed decohenrence in the measurements, calibration of the measurement Hamiltonians.
[11] C. F. Roos, D. Leibfried, A. Mundt, F. Schmidt-Kaler, J. Eschner, and R. Blatt, Phys. Rev. Lett. **85**, 5547 (2000).
[12] D. J. Wineland, C. Monroe, W. M. Itano, D. Leibfried, B. E. King, and D. M. Meekhof, J. Res. Natl. Inst. Stand. Technol. **103**, 259 (1998).
[13] D. Leibfried, R. Blatt, C. Monroe, and D. Wineland, Rev. Mod. Phys. **75**, 281 (2003).
[14] S. Haroche and J.-M. Raimond, *Exploring the Quantum: Atoms and Cavities and Photons* (Oxford University Press, New York, 2006).
[15] Q. A. Turchette, C. J. Myatt, B. E. King, C. A. Sackett, D. Kielpinski, W. M. Itano, C. Monroe, and D. J. Wineland, Phys. Rev. A **62**, 053807 (2000).
[16] D. Kienzler, H.-Y. Lo, B. Keitch, L. de Clercq, F. Leupold, F. Lindenfelser, M. Marinelli, V. Negnevitsky, and J. P. Home, Science **347**, 53 (2015).
[17] W. Schleich, *Quantum Optics in Phase Space* (Wiley, New York, 2001).
[18] Q. A. Turchette, D. Kielpinski, B. E. King, D. Leibfried, D. M. Meekhof, C. J. Myatt, M. A. Rowe, C. A. Sackett, C. S. Wood, W. M. Itano, C. Monroe, and D. J. Wineland, Phys. Rev. A **61**, 063418 (2000).
[19] D. Leibfried, D. M. Meekhof, B. E. King, C. Monroe, W. M. Itano, and D. J. Wineland, Phys. Rev. Lett. **77**, 4281 (1996).
[20] I. Pikovski, M. Zych, F. Costa, and C. Brukner, Nat. Phys. **11**, 668 (2015).
[21] A. Bassi and G. Ghirardi, Phys. Rep. **379**, 257 (2003).
[22] A. Asadian, C. Brukner, and P. Rabl, Phys. Rev. Lett. **112**, 190402 (2014).
[23] S. Ding, G. Maslennikov, R. Hablützel, H. Loh, and D. Matsukevich, arXiv:1512.01670.